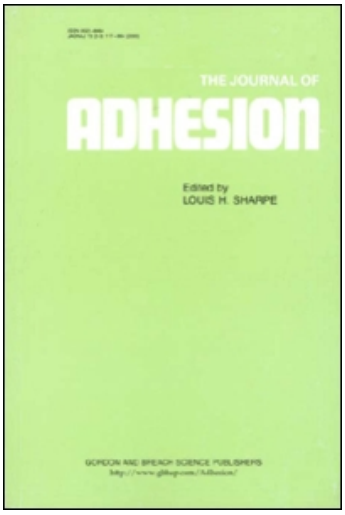

The Journal of Adhesion
Publication details, including instructions for authors and subscription information:
http://www.informaworld.com/smpp/title~content=t713453635

Theoretical and Experimental Analysis of the Scarf Joint Bonded Structure: Influence of the Adhesive Thickness on the Micro-mechanical Behavior

Anthony Objois[a]; Yvon Gilibert[a]; Bernard Fargette[a]
[a] Groupe de Mécanique, Matériaux et Structures (G.M.M.S), Université de Reims Champagne Ardenne, UFR des Sciences Exactes et Naturelles, I.U.T, B.P., Reims Cedex, France

To cite this Article Objois, Anthony , Gilibert, Yvon and Fargette, Bernard(1999) 'Theoretical and Experimental Analysis of the Scarf Joint Bonded Structure: Influence of the Adhesive Thickness on the Micro-mechanical Behavior', The Journal of Adhesion, 70: 1, 13 — 32
To link to this Article: DOI: 10.1080/00218469908010485
URL: http://dx.doi.org/10.1080/00218469908010485

J. Adhesion, 1999, Vol. 70, pp. 13–32
Reprints available directly from the publisher
Photocopying permitted by license only

Theoretical and Experimental Analysis of the Scarf Joint Bonded Structure: Influence of the Adhesive Thickness on the Micro-mechanical Behavior

ANTHONY OBJOIS, YVON GILIBERT* and BERNARD FARGETTE

Groupe de Mécanique, Matériaux et Structures (G.M.M.S),
Université de Reims Champagne Ardenne, UFR des Sciences
Exactes et Naturelles, I.U.T, B.P. 1035, 51687 Reims Cedex 2, France

(Received 2 January 1998; In final form 5 January 1999)

In this work, we have studied the influence of the adhesive thickness on the micro-mechanical behavior of a scarf joint bonded structure loaded in uniaxial tension. Adherends are made of mild steel containing 0.18% Carbon (French Standard XC18), the adhesive is a two-component epoxy resin with a 5800 MPa elastic modulus. The experimental method is based on strain gauge measurements and acoustic emission. It makes it possible to determine the following zones:

- the areas of the joint where the start of microcracks occurs (threshold *Fd*);
- the areas where crack propagation occurs (threshold *Fg*) up to the failure (threshold *Fr*).

The experimental results confirm the good correlation between the different thresholds. They also show that there is an optimal adhesive thickness close to 0.1 mm, which confers to the scarf joint the greatest resistance to microcrack initiation and crack extension. We have compared our experimental measurements with the main theories in this domain to determine their limits and their fields of application, particularly in the angular singularities regions near the ends of the lap.

Keywords: Scarf joint; adhesive thickness; start of microcracks; strain gauge measurements; acoustic emission; asymptotic expansions method

*Corresponding author. Tel.: 03.26.09.27.37, Fax: 03.26.05.30.39.

1. INTRODUCTION

Today, in various industrial sectors, the techniques of assembly by adhesive bonding are superseding the traditional assembly methods such as bolting, welding or riveting. Adhesive bonding has a number of specific advantages, namely, the possibility to assemble different types of materials. The low temperature of the bonding process (room temperature) makes it possible to preserve the atomic arrangement and molecular structure of the substrates. Moreover, the various stages of this process are generally straightforward and so they can be automated. The different studies of the mechanical behavior of bonded structures have led to the creation of shapes which make a more equal distribution of the stresses possible and, thus, a better resistance to the initiation of microcracks during an alternate fatigue test. The ultimate strength of bonded structures does not constitute a safe standard except in the case of a quasi-static increased loading. In fact, the damage to bonded joints starts long before the ultimate break and depends on many well-defined physicochemical factors.

The aim of this study is to characterize the effect of the adhesive thickness on the variation of the micro-mechanical behavior of the scarf joint when it is loaded in uniaxial tension. The substrates are made of a low carbon steel and the adhesive is an epoxy resin. The value of the beveling angle (α) is selected as 33 degrees and we vary the adhesive thickness (*ej*) from 0.05 mm to 1 mm in 0.1 mm increments between 0.1 mm and 1 mm. We determine, for each adhesive thickness, **the global elastic range area, the zones where microcracks are initiated in a steady manner in the joint** and the zones where **the fast propagation of cracks occur up to the final break.**

Our experimental method involves extensometry with electrical gauges and acoustic emission. It makes it possible, on the one hand, to determine the best adhesive thickness which gives the optimal strength and, on the other hand, to compare the theoretical analysis with the real mechanical behavior of the structure.

2. SPECIMEN ELABORATION

2.1. Specimen Reproducibility

Results stemming from experimental analysis are trustworthy only if they involve reliable and reproducible specimens. Besides, good

reliability allows the number of experiments to be limited. To that purpose, we must accurately control all the parameters which act upon the mechanical properties of the bonded structure. The process used to manufacture the specimens, specified in Reference [1], allows us to obtain, for every *ej* value, a constant and homogeneous adhesive thickness along the lap and also a well-defined roughness of the bonding surface. Duplicate tests (3 samples for each thickness) show that reproducibility of specimens and, therefore, of measurements is very good; the standard deviation for the threshold of microcracks, the threshold of flaw propagation and the ultimate level is around 1%.

2.2. Geometry of the Specimen

2.3. Properties of the Specimen Parts

– **The specimen** design is described in Figure 1. It is loaded in uniaxial tension with an universal testing machine. An ISO 12 × 150 thread

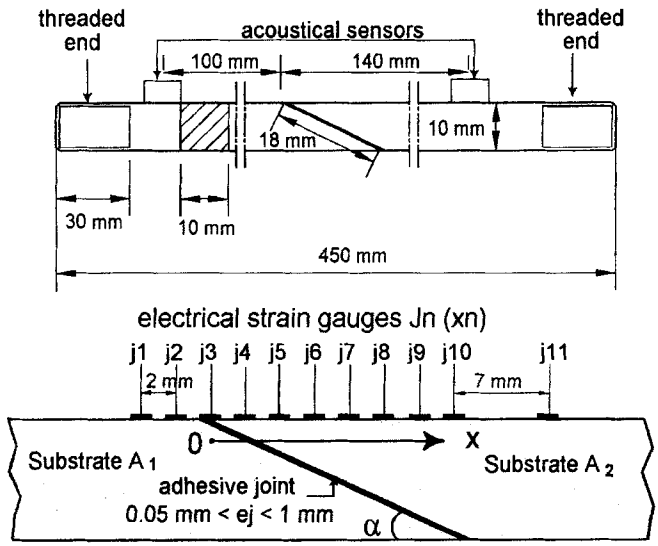

FIGURE 1 Scarf joint bonded structure. Specification of the geometrical shapes and the location of the acoustic cells and the strain gauges.

is machined at each extremity of the specimen in order to screw it into special knee joints which are fitted into the jaws of the testing machine.

- **The adherends** are made of a ferritic steel with 0.18% carbon ("XC 18" French standard). Young's modulus and Poisson's ratio (Tab. I) were determined by using a tensile test with strain gauges. The bars, with a 10 mm × 10 mm square cross section, are first machined by milling and finished with a grinding machine. After that, the extremities are beveled with a 33-degree beveling angle which gives a lap of 18 mm length.
- **The adhesive** is a structural adhesive, EPONAL 317 (commercial name of CECA firm), polymerizing at room temperature (20°C ± 1°C). It is a two-component system: an epoxy resin containing mineral fillers and a hardening agent. We have determined the Poisson's ratio and the Young's modulus (Tab. I) by using a tensile test carried out with a normalized specimen [1, Chap. III]. The curves of applied load *versus* microstrain show an elastic brittle behavior.

2.4. Sand Blasting and Adhesive Bonding

To anchor the adhesive to the substrates, and so to obtain a high quality of bonding, it is necessary to give an optimal roughness to the bonding surface. Previous works have showed that this roughness is obtained, for the adhesive EPONAL 317, by sandblasting with an alumina sand "AVB 150", which has a particle diameter of 95 μm. The sandblasting pressure is about 0.5 MPa, the distance of sandblasting is 10 cm and the sand jet is inclined at 45° from the surface. All these machining operations give to the bonding surface a milling-grinding-sandblasting state, symbolized "M.G.S 150 AVB". The surface profiles, determined with a probe, show that the total roughness, *Rt*, is 11 μm. This latter is close to the average diameter (*dm*) of the adhesive

TABLE I Elastic constant values of the substrates and the adhesive

	Substrates "*XC* 18"	*Adhesive* "*Eponal* 317"
Young's modulus (MPa)	207700	5800
Poisson's ratio	0.29	0.33

mineral fillers ($dm = 7\,\mu m$) and gives the maximal shearing strength to the specimen. In order to prevent the oxidation and the pollution of the surfaces, we bond together the two parts of the specimen immediately after the sandblasting. The two bars, A_1 and A_2, which make up the specimen are put on a V-block fitted with T-slots and tightening screws [2 (1)]. This system leads to a perfect alignment between the substrates and the longitudinal axis. With the help of longitudinal stop screws and a gage foil whose size is equal to the joint thickness, we can accurately adjust the two pieces together with the appropriate joint thickness. After that, a layer of adhesive is spread on the adherends and the bars are lined up and held in this stable position during 30 days at room temperature ($20°C \pm 1°C$), in a vessel where the moisture content is maintained at 40% RH. With this method, we have manufactured specimens whose adhesive thickness (ej) are, respectively: 0.05 mm, 0.1 mm, 0.2 mm, 0.3 mm, 0.4 mm, 0.5 mm, 0.6 mm, 0.7 mm, 0.8 mm, 0.9 mm, 1 mm.

3. THEORETICAL ANALYSIS

3.1. Previous Analysis

The first papers about the theoretical analysis of Single Lap Joints and Double Lap Joints are generally credited to Volkersen [3] and Reissner [4], but it is only with Lubkin's works [5] that we can find the first study of the scarf joint. This latter uses a calculation method based on the plane stress and plane strain hypothesis, and makes the assumption that the adhesive strains are uniform across its thickness. He shows that the distribution of interface stresses is uniform along the joint and is not dependent on the scarf angle, provided that the two adherends have the same elastic properties. Thein's studies [6] allow us to remove this limitation and to take into account the angular singularities at the adherend extremities. All these theoretical analyses show that normal stresses and shear stresses are maximum at the ends of the overlap. However, boundary conditions in the adhesive impose that the shear stresses must become zero at the ends of the lap. In fact, if these analyses give good results in the central part of the lap, they are no longer valid at its ends. Nevertheless, the knowledge of stresses in

these zones is fundamental because they take their highest values there and, experimentally, experience shows that first microcracks start in these places. The asymptotic expansions method developed by Rigolot and Gilibert [7], which consists of adding a corrective stress field, squares with the boundary conditions. So, this theory shows damped exponential singularities near the ends of the lap.

3.2. Assumptions Used in the Analysis and Results Obtained

In this study, we use the theoretical analysis developed by Halfaoui, Klein and Gilibert [8] and Wassiama, Rigolot and Gilibert [9, 10], with the following calculation hypothesis. The adhesive joint is sufficiently far from the ends of the specimen, where the tensile load F is applied, to be able reasonably to make the Saint-Venant assumption. On the perpendicular section of the adherends, the distribution of the normal stresses, σ_0 (Fig. 2), is uniform. Taking into account the transverse sizes of the adherends, in particular their small width as compared with their length, it is reasonable to make the plane strain assumption. This assumption makes it possible to simplify the analysis which, in this way, becomes two-dimensional, and it makes an analytical resolution easier without altering the aptness of the theoretical results. It is assumed that the low carbon steel "XC 18" used for the adherends and the adhesive "EPONAL 317" used for the joint, are homogeneous and isotropic, and their mechanical behaviors are linear elastic. On the adhesive-substrate interfaces, where the strain field and the stress vector are continuous, the adhesiveness between the joint and the substrates is supposed to be perfect. The calculations are based on the plane elasticity hypothesis with a joint loaded in peeling and shearing.

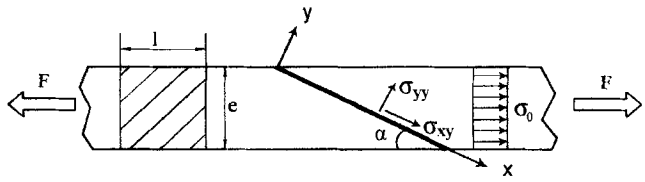

FIGURE 2 Theoretical model. Representation of the boundary conditions.

3.2.1. Superficial Microstrains

In this paragraph, we determine analytically the superficial microstrains (ε_S), parallel to the longitudinal axis of the specimen, along the overlap.

Equation (1), obtained by the Halfaoui theoretical analysis [8], gives the ε_S value *versus* specimen parameters.

$$\varepsilon_S = \frac{F}{e \cdot l \cdot E_S}\left\{1 + \frac{e_J \cdot \cos\alpha}{x\left(\frac{\alpha}{2} + \frac{\sin\alpha}{2}\right)}\left[\left(1 - \frac{E'_J}{E_S}\right)\cos^2\alpha - \nu'_J\left(1 - \frac{E'_J \cdot \nu_S}{\nu'_J \cdot E_S}\right)\sin^2\alpha\right]\right\} \tag{1}$$

With;

ε_S	: superficial microstrain,	E_S	: Young's modulus of the adherends,
F	: tension force,	ν_S	: Poisson's ratio of the adherends,
x	: overlap abscissa,	E_J	: Young's moduli of the hardened adhesive,
e, l	: respectively thickness and width of the specimen,	ν_J	: Poisson's ratio of the hardened adhesive.
α	: scarf angle,		
e_J	: thickness joint,		

In order to improve the agreement between the calculated and the real mechanical behavior, the elastic constants, E_J and ν_J, of the hardened adhesive must be modified; indeed, the plane strain state of the joint, as the Young's modulus of the adherends ($E = 207700$ MPa) is much higher than the Young's modulus of the adhesive ($E = 5800$ MPa), as well as the plane stress assumption concerning the adherends, require the use of corrected values, E'_J and ν'_J:

$$E'_J = \frac{E_J}{1 - \nu_J^2} \quad \text{and} \quad \nu'_J = \frac{\nu_J}{1 - \nu_J}$$

3.2.2. Stresses in the Joint

The calculation of normal (σ_{yy}) and shearing (σ_{xy}) stresses in the joint is worked out in the coordinate system (x, y) (Fig. 2). To that end, we have adapted the relationship established by Wassiama [9]:

$$\begin{cases} \sigma_{xy} = \sigma_0 \sin\alpha\cos\alpha + \sigma^c_{xy}(x,y) \\ \sigma_{yy} = \sigma_0 \sin^2\alpha + \sigma^c_{yy}(x,y) \end{cases} \tag{2}$$

With:

$$\sigma_0 = \frac{F}{e \cdot l},$$

$$\sigma^c_{xy} : \text{corrective shearing stress } \sigma^c_{xy} = -\frac{\partial^2\chi}{\partial x \partial y}(x,y),$$

$$\sigma^c_{yy} : \text{corrective normal stress } \sigma^c_{yy} = \frac{\partial^2\chi}{\partial x^2}(x,y).$$

The Airy function, $\chi(x, y) = e^{-2px} \cdot \pi(y)$ is calculated by the stationary functions method [9], where $\pi(y)$ is the Papkovitch function which is associated with the complex number, p, solution of the complex equation: $p - (3 + 4\nu)\sin(p) = 0$.

$\chi(x, y)$ is given by the following expression:

$$\chi(x,y) = 2B\{e^{-2px}[K\cos[p(2y-1)] + (2y-1)\sin[p(2y-1)]]\}$$

The B and K constants depend on the geometrical and mechanical properties of the specimen and they are given by the following equations:

$$K = \frac{2(1-\nu_J) - (3+4\nu_J)\sin^2\left(\frac{p}{2}\right)}{p} \quad \text{and}$$

$$B = \frac{\left[-\frac{\nu_J}{1-\nu_J}\sin^2\alpha + \cos^2\alpha\right]\sigma_0}{8p(2-Kp)}$$

In the middle of the joint:

$$\sigma^c_{xy} = \sigma^c_{yy} = 0, \text{ so } \begin{cases} \sigma_{xy} = \sigma_0 \sin\alpha\cos\alpha \\ \sigma_{yy} = \sigma_0 \sin^2\alpha \end{cases} \tag{3}$$

The analysis of the expressions (2) shows that the normal stresses (σ_{yy}) and shearing stresses (σ_{xy}) are uniform on the major part of the lap and they are maximal towards the extremities.

4. EXPERIMENTAL METHOD

The experimental method is based on strain gauge measurements and acoustic emission during a slow tensile test at room temperature ($20°C \pm 1°C$).

4.1. Microstrain Measurements with Electrical Strain Gauges

Strain measurements inside the joint cannot be obtained directly; therefore, we used electrical strain gauges located at different points on the external surfaces of the metallic adherends. When a bonded assemblage is loaded in tension, apart from the areas near the beveled extremities, the mechanical behavior of the adherends remains in the elastic range. So, if a microcrack occurs in the joint, the microstrain field measured along the outer surface of the adherends, just above the microcrack, is perturbed. So, for each strain gauge, a change in the slope or a change in the sign of the curve ($dF/d\varepsilon$) of "applied load" *versus* "microstrain" shows a microcrack initiation or a flaw propagation within the adhesive underneath this point [11, 12]. So, the extensometric method with strain gauges is able to follow indirectly the process of damage to the bonded joint. In order to measure accurately the microstrain along the lap, the electrical strain gauges (grouped in a strip gauge) are located along the longitudinal axis at different points (with a 2 mm step) on the external surfaces of adherends. The strip gauge position and the abscissas, x_n (in millimeters), of the gauges' centers, $J_n(x_n)$, are shown in Figure 1.

4.2. The Acoustic Emission

The acoustic emission (AE) can be defined as a sonorous wave production, emitted in salvos, caused by a sudden energy release in the

tensioned material during its damage [13]. So, when the tensile load exceeds the proportional limit of the adhesive, the relaxation of stress due to the initiation of microcracks, the growth of cracks or the propagation of flaws, cause a sudden increase in acoustic activity up to the ultimate break. If the specimen is made of brittle adhesive and metallic adherends, each distinctive step of the joint' damage causes a significant increase in the acoustic emission.

4.3. Experimental Analysis

Tensile tests are carried out at a very low strain rate ($5\,\mathrm{N}\cdot\mathrm{sec}^{-1}$) at room temperature. The specimen is fitted out with strain gauges and acoustic emission sensors, put at well-defined points (Fig. 1).

We have three or four similar specimens for every adhesive thickness (*ej*) in case they are needed. The use of strip gauges is not easy and is particularly expensive; this is why, for each thickness value, only one assemblage is equipped with strip gauges, the others are only provided with acoustic sensors. The latter are put on the specimen and connected to a spectrum analyzer when the assemblage is fitted into the jaws of the testing machine. In order to prevent interference by noises coming from the hydraulic system and the special knee joints, the sonorous waves in a range below 35 dB are not recorded. The strain gauges are connected to a computer system which analyses and records the data. The acoustical spectrum and the microstrains are simultaneously recorded during all the tensile test duration.

4.4. Determination of the Thresholds Fd_n, Fg_n and Analysis of the Curves $F = f(\varepsilon)$ and $NC = f(F)$

For every tested specimen, the determination of the damage thresholds of the bonded structure is based on analysis of the curve $F = f(\varepsilon)$: applied load F *versus* microstrain ε. In order to back up this analysis, we also use acoustic measurements, particularly the curve $NC = f(F)$, which shows the number of acoustic events *versus* applied load. Figure 3 shows the curves $F = f(\varepsilon)$ and $NC = f(F)$ related to the specimen with a 0.3 mm adhesive thickness. It is very interesting to note that the extensometric method is closely related to the acoustic analysis. During the first part of the tensile test, from $F = 0$ to $F = 4.32\,\mathrm{kN}$, the linear

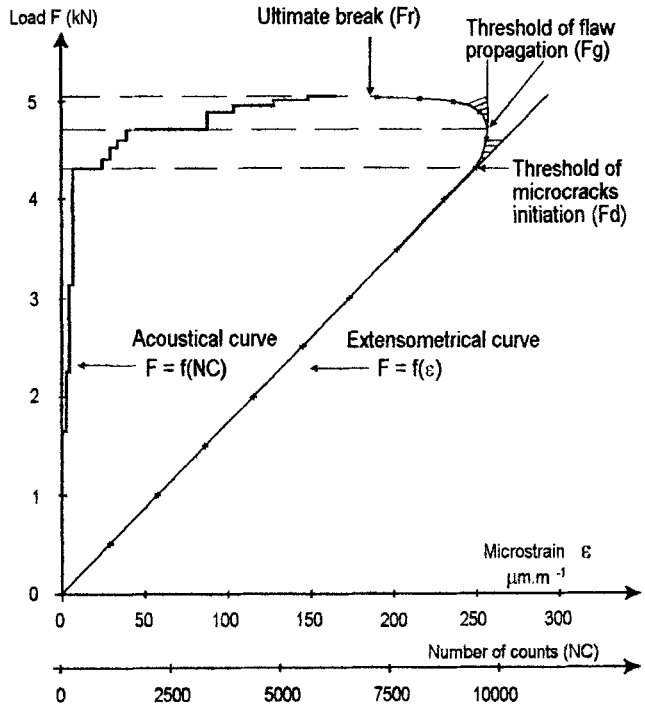

FIGURE 3 Representation of the extensometric curve $F = f(\varepsilon)$ and the acoustic curve $NC = f(F)$. The adhesive joint is 0.3 mm thick and the microstrains are recorded by the $J_5(x_5 = 4\,\text{mm})$ gauge.

variation of strains, measured with the gauges, is indicative of the elastic behavior of the specimen. The first microcracks start in the joint for a 4.32 kN load and they cause a change in the slope of the curve $F = f(\varepsilon)$. This start of microcracking is also backed up by the first sudden increase of the acoustic emission on the curve $NC = f(F)$. Afterwards, the decrease of strain (change in the sign of $dF/d\varepsilon$), caused by the relaxation of stresses in the adherends and the second fast increase in acoustical activity, point to the flaw propagation in an unsteady manner within the adhesive. The break occurs for a 5.04 kN load. So, for each gauge, $J_n(x_n)$ ($n = 1$ to 11), located along the overlap, we can determine the following thresholds:

- $\mathbf{Fd}_n$: threshold of microcrack initiation under the gauge $J_n(x_n)$ which corresponds to the proportional limit of the zone tested by this gauge.

- Among the Fd_n values, the minimal one points to the upper limit, Fd, of the "global elastic range" of the specimen.
- **Fg$_n$**: threshold of flaw propagation under the gauge $J_n(x_n)$, characterized by a change in sign of the slope, $dF/d\varepsilon$. Beyond this limit, microcracks join to form macroscopic cracks which extend, in an unsteady manner, within the adhesive layer up to breaking point.
- **Fr**: threshold of the ultimate break.

4.5. Analysis of the Curves $F = f(\varepsilon)$ Along the Lap

The gauges $J_{11}(x_{11} = 21\,\text{mm})$, located far from the beveled point (Fig. 1), $J_1(x_1 = -4\,\text{mm})$, $J_2(x_2 = -2\,\text{mm})$ and located on the bulky part of the substrate, show a linear variation of the microstrains up to the ultimate break (Fig. 4). These curves are indicative of the elastic behavior of the metallic adherends ($E = 207700\,\text{MPa}$). It is not easy to analyze the strain measured by $J_3(x_3 = \text{mm})$, because this gauge records both the strains of the adhesive and the metallic adherends. Moreover, in this area the proportional limit of the metal is quickly reached because of the high overstresses due to the edge effects. The zone under the $J_4(x_4 = 2\,\text{mm})$ gauge shows a linear behavior up to a 4.4 kN load; after that, a nonlinear behavior is noted up to the break ($F = 5.04\,\text{kN}$). The curves $F = f(\varepsilon)$ relating to the following gauges:

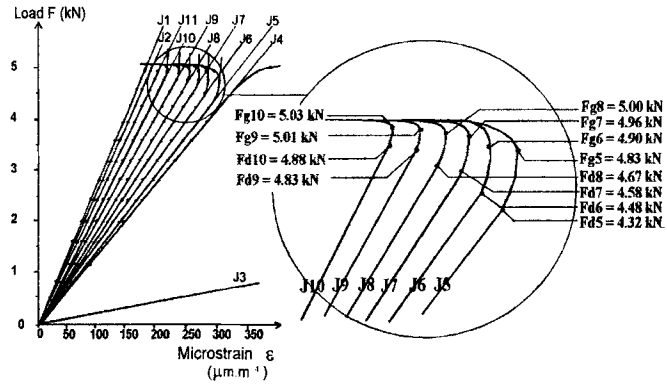

FIGURE 4 Extensometric curves of applied load, F, *versus* microstrain, ε, along the lap. Influence of the gauge position. The adhesive joint is 0.3 mm thick.

$J_5(x_5 = 4\,\text{mm}), J_6(x_6 = 6\,\text{mm}), J_7(x_7 = 8\,\text{mm}), J_8(x_8 = 10\,\text{mm}), J_9(x_9 = 12\,\text{mm}), J_{10}(x_{10} = 14\,\text{mm})$ located along the lap, show similar global lines, namely: a **linear part** which is indicative of the elastic behavior of the specimen and a **non-linear part** which is characteristic of the damage stage of the adhesive joint.

So, it is with these curves $F = f(\varepsilon)$ (with $0\,\text{kN} \leq F \leq Fr = 5.04\,\text{kN}$) relating to the gauges $J_n(x_n)$ ($n = 5$ to 10), that we determine the variations of the thresholds Fd_n, Fg_n and Fr along the lap. In this way, the graphic representation of them (Fig. 5) makes it possible to show the various ranges of the **micro-mechanical behavior** of the specimen.

5. COMPARISON BETWEEN EXPERIMENTAL AND THEORETICAL RESULTS

The theory-experiment comparison is made with the superficial microstrains (ε_S) along the longitudinal axis of the lap.

The curves in Figure 6 show the comparison between the theoretical microstrains (ε_S) calculated with Eq. (1) and the experimental values measured with strain gauges for increasing loads (2 kN, 3 kN, 5 kN) along the lap, with a joint 0.3 mm thick.

In the same way, we compare (Fig. 7), for all the thicknesses ($ej = 0.05$ mm to 1 mm), the microstrains measured and computed (for

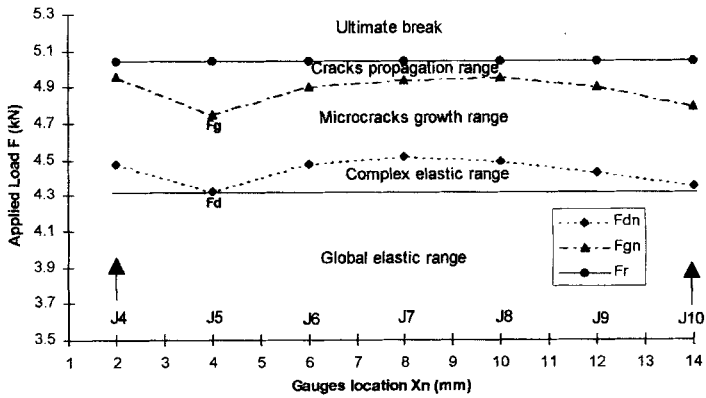

FIGURE 5 Representation of the scarf joint damage ranges along the lap. The adhesive joint is 0.3 mm thick.

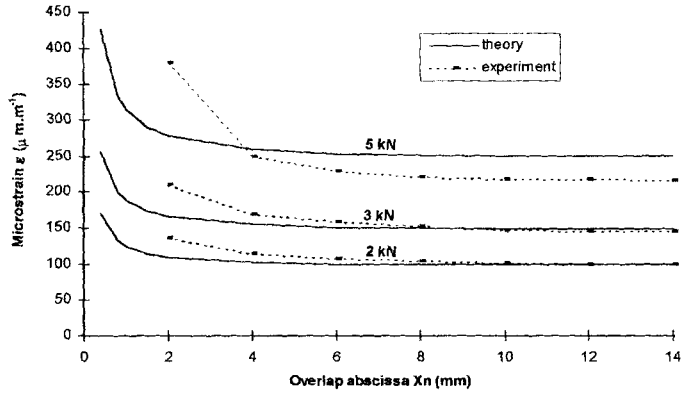

FIGURE 6 Comparison between theoretical values and longitudinal microstrains measured at the outer surface of adherends, for three applied loads (2 kN, 3 kN, 5 kN). The adhesive joint is 0.3 mm thick and $Fd = 4{,}32$ kN.

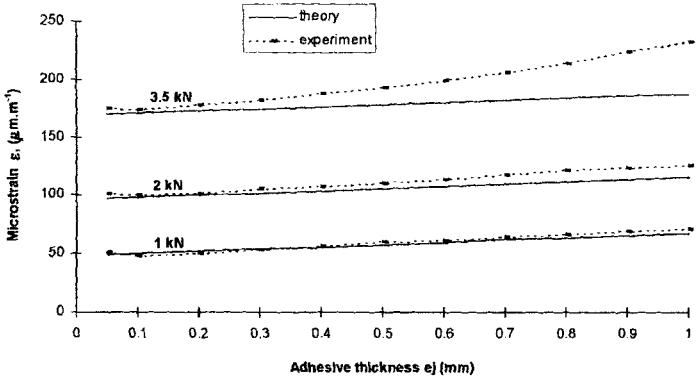

FIGURE 7 Comparison, for increasing loads, between the microstrains measured and the values computed at the abscissa $x_5 = 4$ mm. $ej = 0.05$ mm to 1 mm.

increasing loads) at the abscissa $x_5 = 4$ mm, where the first damage in the joint starts.

These comparisons (Figs. 6, 7) emphasize the difficulty in anticipating the micro-mechanical behavior of bonded structures with only theoretical analysis. In fact, the latter can be used only in very specific conditions. Indeed, near the ends ($0 < x_n < 4$ mm), where the elastic limit is quickly reached, the curves $\varepsilon_S = f(x_n)$ (Fig. 6) show a growing deviation between the theoretical and the experimental microstrains.

Nevertheless, the theory is in accordance with experience on the main part of the lap ($x_n > 4$ mm), provided the applied load F is much lower than the elastic limit ($F < Fd$) of the specimen. After that, as soon as the level Fd is exceeded, a growing deviation occurs between computed values and experimental microstrains. A similar phenomenon in shown on Figure 7 which shows the ε_S variation *versus* the adhesive thickness at the abscissa $x_5 = 4$ mm. The agreement between theory and test is satisfactory if the tensile load is lower than the upper limit (Fd) of the global elastic range. Indeed, when the threshold Fd is exceeded, the mechanical behavior rapidly becomes complex because the microcracked zones coexist and react with the non-cracked elastic zones within the adhesive. The theoretical model can no longer predict the non-linear mechanical behavior of a damaged specimen.

6. SPECIMEN MICRO-MECHANICAL BEHAVIOR ANALYSIS

6.1. Characterization of the Damage α Scarf Joint

For all the specimens, the start of the first microcracks and flaw propagation in an unsteady manner, respectively characterized by the Fd and Fg thresholds, occurs near the ends of the beveled adherends under the gauge $J_5(x_5 = 4\,\text{mm})$. Beyond the global elastic range, the microcracks extend step-by-step when the applied load, F, increases. Microcracking occurs symmetrically at the other beveled extremity. Nevertheless, the gauges located on the opposite surface are further away: so, the elastic field perturbations occur at the same level, but with a lower intensity on the curves $F = f(\varepsilon)$. Our results show that the joint damage, brought about stress concentration, starts near the beveled extremities and extends towards the middle of the lap. On the other hand, the growth and propagation of microcracks to the ends are much slower because the local plastic flow of the metal in this zone makes it possible for the stresses to relax. So, the mechanical strength of the "scarf joint" depends in large part of the behavior of the adhesive near the joint ends. Nevertheless, unlike bonded structures having strong angular singularities such as tenon-and-mortise joints or double-lap joints, [14, 1, 15], the elastic limit of the scarf joint is reached for a tensile load (Fd) close to the ultimate failure

load, *Fr* (*Fd* ≅ 80% of *Fr*). We explain that by the geometrical configuration of the joint, in particular the line-up of the beveled shape of the substrates (A_1 and A_2), which avoids the bending effect involved in a rotating joint and makes possible uniform distribution of the stresses on the main part of the lap. This feature is especially interesting when the structure is loaded in fatigue. Indeed, previous studies [8, 12], [2 (3)], involving alternate tensile tests with a scarf joint, have shown that the useful life of a **non-damaged** specimen is nearly infinite; whereas, in the same conditions, the ultimate failure occurs after only 40,000 cycles if the specimen has previously been damaged by preloading over the *Fd* level.

6.2. Influence of the Adhesive Thickness Value

The experimental method used to manufacture the specimens [2 (1)], allows us to obtain a constant thickness (*ej*) of the adhesive layer over the whole length of the lap. We studied the following values of *ej*: 0.05 mm, 0.1 mm, 0.2 mm, 0.3 mm, 0.4 mm, 0.5 mm, 0.6 mm, 0.7 mm, 0.8 mm, 0.9 mm, 1 mm. The adhesive is too viscous to obtain a joint thickness less than 0.05 mm.

For each thickness, three tensile tests are carried out with a $5\,N \cdot sec^{-1}$ load rate ($\dot{\varepsilon} = 133 \cdot 10^{-9}\,sec^{-1}$). So, we determine, with the specimen fitted with gauges, the threshold **Fd** of the **first** microcracks, the threshold **Fg** of the flaw propagation and the threshold *Fr* of the ultimate break. Our measurements show that the early values of these thresholds (symbolized by *Fd* and *Fg*), which correspond to the **first** damage levels of the specimen, are all detected for each specimen, at the abscissa $x = 4$ mm (gauge J_5) (Fig. 4). The Table II shows the values of the *Fd* and *Fg* thresholds and the ultimate strength, *Fr*, for each adhesive thickness.

TABLE II Variation of the thresholds of **first** damage (*Fd*, *Fg*) and ultimate strength (*Fr*) *versus* the adhesive thickness (*ej*)

ej (*mm*)	**0.05**	**0.1**	**0.2**	**0.3**	**0.4**	**0.5**	**0.6**	**0.7**	**0.8**	**0.9**	**1**
Fd (kN)	3.83	4.81	4.38	4.32	4.1	4	3.81	3.62	3.51	3.42	3.14
Fg (kN)	4.06	5.08	4.83	4.75	4.7	4.65	4.51	4.4	4.19	3.92	3.79
Fr (kN)	4.21	5.3	5.18	5.04	4.95	4.87	4.65	4.54	4.43	4.02	3.92

Figure 8 shows, on the one hand, the thresholds *Fd*, *Fg* and *Fr* are related among themselves and, on the other hand, the value of the adhesive thickness acts substantially upon the levels of microcracks initiation, flaw propagation and ultimate break. There is an optimal thickness, close to 0.1 mm, which gives the maximum mechanical strength to the structure; $Fd = 4.81$ kN; $Fg = 5.08$ kN and $Fr = 5.3$ kN. Beyond this optimal thickness, the thresholds decrease step-by-step until the following values; $Fd = 3.14$ kN; $Fg = 3.79$ kN and $Fr = 3.92$ kN, for $ej = 1$ mm. We think that this decrease of the mechanical strength of the specimen is caused by the growing overstresses within the adhesive near the ends of the joint when *ej* increase. Indeed, the measurements carried out with the gauges near the beveled extremities show that the microstrains and, therefore, the stresses, are more and more significant in this zone, when the thickness of the joint increases. We explain these overstresses by the growing heterogeneity in the mechanical behavior of the joint area which is made up of a **brittle** adhesive layer and very **stiff** adherends ($E = 207700$ MPa). Moreover, Figure 8 shows that the mechanical strength of the specimen decreases suddenly when *ej* is lower than 0.1 mm. Indeed, a joint which is too thin makes impossible an optimal distribution [16] of the stresses within the adhesive layer.

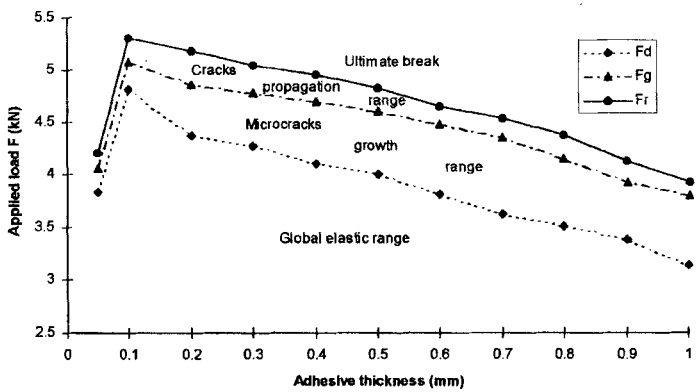

FIGURE 8 Influence of the adhesive thickness (*ej*) on the thresholds *Fd*, *Fg* and *Fr*.

7. CONCLUSION

It is always difficult to analyze the micro-mechanical behavior of bonded structures. The experimental techniques are expensive, difficult to apply and the results are accurate only if they involve reliable and reproducible specimens (mechanical properties of adherends and adhesive, surface condition and geometrical factors). This work shows that rupture strength of bonded structures does not constitute a safe criterion. Indeed, microcracks start and spread along the adhesive joint at loads less than the ultimate (*Fr*). Among all the thresholds which characterize this gradual damage, we consider the threshold (**Fd**) of the **first** microcracks initiation as the **fundamental parameter**. Indeed, the *Fd* threshold marks the end of the elastic behavior of the bonded structure and it also corresponds to the level of reversibility. It is interesting to notice that, for all the specimens which have been studied, the initiation of the first microcracks, simultaneously detected with strain gauges and acoustic emission, occur near the extremities of the joint. After that, when the tensile load F increases, the microcracks grow and spread much more quickly towards the central part of the joint than towards its ends because extremities of the substrates fit to the stress concentration. The theoretical analysis is consistent with the real mechanical behavior of the specimens in the global elastic range. Moreover, in this range and for every adhesive thickness, theory shows that shear stress is maximum near the ends of the lap. During a uniaxial loading test with a specimen in which the scarf angle is optimal ($\alpha \cong 30°$), the shearing stresses, due to the relative displacement of the adherends along the bond, are predominant within the adhesive joint; the geometrical shape of the joint gives it a high elastic limit. Whatever the adhesive thickness, damage occurs at a tensile load, F, close to the breaking load ($F \cong 80\%$ of *Fr*). This is why this bonded structure has a high fatigue strength. To our knowledge, it is the first time that an experimental analysis of the scarf joint, with the simultaneous use of strain gauges and acoustic emission, shows that there is an optimal adhesive thickness, which gives the structure the greatest resistance to the initiation and the extension of microcracks. For every adhesive thickness, the threshold of microcrack initiation (Fd_n) the threshold of flaw propagation (Fg_n) and the threshold of the ultimate break (*Fr*) are linked. Taking into account the bonding

process of a brittle adhesive whose viscosity in the non-hardened state is high, our research shows that the optimal practical mechanical strength of the scarf joint can be obtained by an adhesive thickness in the range of 0.1 mm – 0.2 mm. As far as a very fluid non-hardened adhesive is concerned, the optimal strength could be obtained with a thinner layer of adhesive, in the region of 0.1 mm.

References

[1] Gilibert, Y., "Contribution à l'étude de l'adhésivité de matériaux collés par l'intermédiaire de résines époxydiques", *Thèse de Doctorat ès Sciences Physiques, Université de Reims* (1978).

[2] Gilibert, Y. (1) "Procédé d'assemblage par collage de deux substrats aboutés". French Patent no. 87.15575, European Patent no. 88.402835.8. (2) "Dispositif d'ancrage mécanique pour le maintien d'une extrémité d'une pièce parallélépipédique, procédé de fabrication d'un tel dispositif et adaptateur pour son montage sur une machine de traction". French Patent no. 86.14137, European Patent no. 2.605.068. (3) "Procédé pour augmenter la résistance mécanique à la formation de microfissures dans un joint adhésif structural ou dans une masse de multimatériaux". French Patent no. 88.04094.

[3] Volkersen, O., "Die Nietkraftverteilung in zugbeanspruchten Neitverbindungen mit konstanten Laschenquerschnitten", *Luftfahrtforschung* **15**, 41 (1938).

[4] Goland, M. and Reissner, E., "The stresses in cemented joints", *J. Applied Mech.* **11**, A-17 (1944).

[5] Lubkin, J. L., "A theory of adhesif scarf joint", *J. Applied Mech.* **255** (1957).

[6] Thein, Wah, "Plane stress analysis of a scarf joint", *Int. J. Solids Structures* **12**, 491 (1976).

[7] Rigolot, A. and Gilibert, Y., "Théorie élastique de l'assemblage collé", *RILEM, Matériaux et Constructions*, Dunod Editeur, France **107**, 363 (1985).

[8] Gilibert, Y., Halfaoui, S. and Klein, M. L. L., "Influence de la rugosité sur le comportement mécanique fin en traction statique et en fatigue par traction ondulée de l'assemblage collé en sifflet", *XX^{ème} Congrés FATIPEC*, Nice (1990), Published in Congress Proceeding, pp. 309 – 324.

[9] Wassiama, A., "Analyse théorique et expérimentale des contraintes dans un assemblage collé à simple recouvrement en biseau", *Thèse de Doctorat de l' Université de Paris VI* (1991).

[10] Gilibert, Y., Rigolot, A. and Wassiama, A., "Singularité des contraintes dans les assemblages collés en biseau", *EUROCOAT 91, XIXè Congrés de l'A.F.T.P.V.*, Nice (1991). Comptes rendus du colloque, pp. 245 – 252, published by EREC Puteaux, France; and in review *DOUBLE LIAISON* **38**, 32 (1991).

[11] Gilibert, Y., Komiha, M. A., Rigolot, A. and Verchery, G., "Analyse théorique et expérimentale de l'influence de l'épaisseur du film de colle, dans un assemblage collé à double recouvrement", *C.R. des Journées Universitaires Genie Civil*, E.N.S.E.T., Cachan, France (1984).

[12] Mekiri, L., "Contribution à l'étude du comportement mécanique fin de l'assemblage à simple recouvrement du type sifflet, sollicité en traction simple et en fatigue", *Thèse de Doctorat de l'Université de Paris VI* (1991).

[13] Stone, D. E. W. and Dingwall, P. F., "Acoustic emission parameters and their interpretation", *NDT International* **10**, 51 (1977).

[14] Fargette, B., Gilibert, Y. and Rimlinger, L., "Comparison between experimental and theoretical analysis of stress distribution in adhesively-bonded joints: Tenon and Mortise Joints and Single-Lap Joints", *J. Adhesion* **59**, 159 (1996).
[15] Ishal, O. and Gali, S., "Two-dimensional interlaminar stress distribution within the adhesive layer of a symmetrical doubler model", *J. Adhesion* **8**, 301 (1977).
[16] Komiha, M. A., "Analyse théorique et expérimentale de l'influence de l'épaisseur du film de colle dans un assemblage collé à double recouvrement", *Thèse de Doctorat de l'Université de Paris VI* (1983).